The Astronomical Journal, 133:1934–1946, 2007 May

LATE-TYPE NEAR-CONTACT ECLIPSING BINARY [HH97] FS AUR-79

S. J. Austin
Department of Physics and Astronomy, University of Central Arkansas, Conway, AR 72035, USA; saustin@uca.edu

J. W. Robertson
Department of Physical Sciences, Arkansas Tech University, Russellville, AR 72801-2222, USA; jeff.robertson@atu.edu

C. Tycner[1,2]
US Naval Observatory, Flagstaff Station, Flagstaff, AZ 86001-8521, USA; tycner@sextans.lowell.edu

T. Campbell
Whispering Pines Observatory, Harrison, AR 72601, USA; jmontecamp@yahoo.com

and

R. K. Honeycutt
Department of Astronomy, Indiana University, Bloomington, IN 47405, USA; honey@astro.indiana.edu
Received 2006 November 9; accepted 2007 January 6

ABSTRACT

The secondary photometric standard star number 79 for the FS Aur field (Henden & Honeycutt 1997), designated as [HH97] FS Aur-79 (GSC 1874−399), is a short-period (0.2508 days) eclipsing binary whose light curve is a combination of the β Lyr and BY Dra type variables. High signal-to-noise ratio multicolor photometry was obtained using the US Naval Observatory 1 m telescope. These light curves show asymmetry at quadrature phases (the O'Connell effect), which can be modeled with the presence of starspots. A low-resolution spectrum obtained with the 3.5 m Wisconsin-Indiana-Yale-NOAO telescope at orbital phase 0.76 is consistent with a spectral type of dK7e and dM3e. A radial velocity curve for the primary star was constructed using 24 high-resolution spectra from the 9.2 m Hobby-Eberly Telescope. Spectra show Hα and Hβ in emission confirming chromospheric activity and possibly the presence of circumstellar material. Binary star models that simultaneously fit the *U*, *B*, *V*, *R*, and radial velocity curves are those with a primary star of mass $0.59 \pm 0.02\ M_{\odot}$, temperature 4100 ± 25 K, and mean radius $0.67\ R_{\odot}$, just filling its Roche lobe, and a secondary star of mass $0.31 \pm 0.09\ M_{\odot}$, temperature 3425 ± 25 K, and mean radius $0.48\ R_{\odot}$, just within its Roche lobe. An inclination angle of $83^{\circ} \pm 2^{\circ}$ with a center-of-mass separation of $1.62\ R_{\odot}$ is also derived. Starspots, expected for a rotation period of less than 1 day, had to be included in the modeling to fit the O'Connell effect.

Key words: binaries: close — binaries: eclipsing — binaries: spectroscopic — stars: late-type

1. INTRODUCTION

Henden & Honeycutt (1997) designated this star as the 79th standard star in the field of cataclysmic variable star FS Aur; this star is also cataloged GSC 1874−399 in the Guide Star Catalog and misreferenced as [HH95] FS-79 by SIMBAD,[3] although it should be [HH97] FS-79. In this paper we refer to this star as FS Aur-79. The discovery that this star was actually an eclipsing binary was described by Robertson et al. (2004). They found that the orbital period was approximately 0.25 days and that the temperatures of the two stars were not equal, indicating that the two stars were not in contact. Their low signal-to-noise ratio (S/N) *BVR* photometry from 2003–2004 enabled them to determine preliminary system parameters such as mass ratio, inclination angle, effective temperatures, and filling factors. This indicated a near-contact binary system with late-type components.

Good, accurate, fundamental parameters for late-type main-sequence stars are based on only a handful of double-lined spectroscopic, totally eclipsing binaries with K and M components. Therefore, there are considerable gaps in our interpolations and knowledge. This is also true when determining effective temperature for cooler M dwarfs, as the complexity of molecules present in their atmospheres increases with later spectral types. Near-contact and contact systems with these very late components are extremely rare and are therefore interesting for what they can tell us about binary stellar formation and evolution.

To better constrain the system parameters we obtained high S/N *UBVR* photometry and spectra to determine the radial velocity curves. In § 2 we describe how the photometry and spectroscopy were obtained and reduced. In § 3 we present the photometric and spectroscopic analysis. Section 4 is a discussion of our results, and § 5 is a summary of our conclusions.

2. OBSERVATIONS AND REDUCTIONS

2.1. *Photometry*

2.1.1. *Center for Backyard Astrophysics Photometry*

After the initial discovery of this eclipsing variable star (Robertson et al. 2004), additional light curves were collected by T. C. on 15 nights from 2003 November through 2004 February. The interest of the Center for Backyard Astrophysics (CBA) in the cataclysmic variable FS Aur, very near our newly discovered variable, also helped spark a professional-amateur observational campaign by some members of the CBA to collect differential photometry for obtaining times of eclipse minima. Data were gathered by T. C. (CBA-Arkansas), T. Krajci (2006; CBA-New Mexico), P. de Ponthiere (CBA-Lesve), and J. Foote (CBA-Utah) on 45 nights from 2005 October to 2006 January. Details of the observatories and their telescope/detector configurations can

[1] Michelson Postdoctoral Fellow.
[2] Also at NVI, Inc., Greenbelt, MD 20770, USA.
[3] The SIMBAD database is maintained by the CDS, Strasbourg, France.

Report Documentation Page

Form Approved
OMB No. 0704-0188

1. REPORT DATE	2. REPORT TYPE	3. DATES COVERED
MAY 2007		**00-00-2007 to 00-00-2007**

4. TITLE AND SUBTITLE	5a. CONTRACT NUMBER
Late-Type Near-Contact Eclipsing Binary [HH97], FS AUR-79	5b. GRANT NUMBER
	5c. PROGRAM ELEMENT NUMBER
6. AUTHOR(S)	5d. PROJECT NUMBER
	5e. TASK NUMBER
	5f. WORK UNIT NUMBER
7. PERFORMING ORGANIZATION NAME(S) AND ADDRESS(ES) **US Naval Observatory,Flagstaff Station,Flagstaff,AZ,86001-8521**	8. PERFORMING ORGANIZATION REPORT NUMBER
9. SPONSORING/MONITORING AGENCY NAME(S) AND ADDRESS(ES)	10. SPONSOR/MONITOR'S ACRONYM(S)
	11. SPONSOR/MONITOR'S REPORT NUMBER(S)

12. DISTRIBUTION/AVAILABILITY STATEMENT
Approved for public release; distribution unlimited

13. SUPPLEMENTARY NOTES

14. ABSTRACT

15. SUBJECT TERMS

16. SECURITY CLASSIFICATION OF:			17. LIMITATION OF ABSTRACT	18. NUMBER OF PAGES	19a. NAME OF RESPONSIBLE PERSON
a. REPORT	b. ABSTRACT	c. THIS PAGE			
unclassified	**unclassified**	**unclassified**	**Same as Report (SAR)**	**13**	

TABLE 1
CBA Times of Minimum

HJD	Phase Cycle	Filter	Observatory
2,452,963.74445.....	0.0	*R*	CBA-Arkansas
2,452,963.86918.....	0.5	*R*	CBA-Arkansas
2,452,964.74756.....	4.0	*R*	CBA-Arkansas
2,452,964.87062.....	4.5	*R*	CBA-Arkansas
2,452,965.75061.....	8.0	*R*	CBA-Arkansas
2,452,966.00206.....	9.0	*R*	CBA-Arkansas
2,452,968.76013.....	20.0	*R*	CBA-Arkansas
2,452,971.89528.....	32.5	*R*	CBA-Arkansas
2,452,972.77382.....	36.0	*R*	CBA-Arkansas
2,452,984.68797.....	83.5	*V*	CBA-Arkansas
2,452,984.81383.....	84.0	*V*	CBA-Arkansas
2,452,985.68966.....	87.5	*V*	CBA-Arkansas
2,452,985.81665.....	88.0	*V*	CBA-Arkansas
2,452,988.70157.....	99.5	*V*	CBA-Arkansas
2,452,988.82615.....	100.0	*V*	CBA-Arkansas
2,452,990.71092.....	107.5	*V*	CBA-Arkansas
2,452,990.83218.....	108.0	*V*	CBA-Arkansas
2,452,991.70918.....	111.5	*V*	CBA-Arkansas
2,452,991.83667.....	112.0	*V*	CBA-Arkansas
2,452,992.71317.....	115.5	*V*	CBA-Arkansas
2,452,992.83898.....	116.0	*V*	CBA-Arkansas
2,453,032.71822.....	275.0	*B*	CBA-Arkansas
2,453,033.72253.....	279.0	*B*	CBA-Arkansas
2,453,035.72843.....	287.0	*B*	CBA-Arkansas
2,453,691.86440.....	2903.0	none	CBA-NM[a]
2,453,691.98820.....	2903.5	none	CBA-NM[a]
2,453,693.87070.....	2911.0	none	CBA-NM[a]
2,453,693.99380.....	2911.5	none	CBA-NM[a]
2,453,694.87390.....	2915.0	none	CBA-NM[a]
2,453,694.99770.....	2915.5	none	CBA-NM[a]
2,453,695.75052.....	2918.5	none	CBA-Utah
2,453,695.87817.....	2919.0	none	CBA-Utah
2,453,696.00030.....	2919.5	none	CBA-NM[a]
2,453,696.00045.....	2919.5	none	CBA-Utah
2,453,696.88030.....	2923.0	none	CBA-NM[a]
2,453,697.75706.....	2926.5	none	CBA-Utah
2,453,697.88463.....	2927.0	none	CBA-Utah
2,453,698.00781.....	2927.5	none	CBA-Utah
2,453,700.89360.....	2939.0	none	CBA-NM[a]
2,453,701.01730.....	2939.5	none	CBA-NM[a]
2,453,702.89960.....	2947.0	none	CBA-NM[a]
2,453,703.77660.....	2950.5	none	CBA-NM[a]
2,453,703.90330.....	2951.0	none	CBA-NM[a]
2,453,704.77960.....	2954.5	none	CBA-NM[a]
2,453,704.90620.....	2955.0	none	CBA-NM[a]
2,453,705.77857.....	2958.5	none	CBA-Utah
2,453,705.78390.....	2958.5	none	CBA-NM[a]
2,453,705.90960.....	2959.0	none	CBA-NM[a]
2,453,705.91027.....	2959.0	none	CBA-Utah
2,453,706.78640.....	2962.5	none	CBA-NM[a]
2,453,706.91310.....	2963.0	none	CBA-NM[a]
2,453,708.79220.....	2970.5	none	CBA-Utah
2,453,708.92054.....	2971.0	none	CBA-Utah
2,453,709.79660.....	2974.5	none	CBA-NM[a]
2,453,709.92290.....	2975.0	none	CBA-NM[a]
2,453,710.79990.....	2978.5	none	CBA-NM[a]
2,453,710.92600.....	2979.0	none	CBA-NM[a]
2,453,711.80206.....	2982.5	none	CBA-Utah
2,453,711.80320.....	2982.5	none	CBA-NM[a]
2,453,711.92940.....	2983.0	none	CBA-NM[a]
2,453,711.93056.....	2983.0	none	CBA-Utah
2,453,712.80650.....	2986.5	none	CBA-NM[a]
2,453,712.93250.....	2987.0	none	CBA-NM[a]
2,453,713.80960.....	2990.5	none	CBA-NM[a]
2,453,713.93600.....	2991.0	none	CBA-NM[a]
2,453,716.44484.....	3001.0	none	CBA-Lesve
2,453,719.83070.....	3014.5	none	CBA-NM[a]
2,453,719.95590.....	3015.0	none	CBA-NM[a]
2,453,725.59880.....	3037.5	none	CBA-NM[a]
2,453,725.72410.....	3038.0	none	CBA-NM[a]
2,453,725.84950.....	3038.5	none	CBA-NM[a]
2,453,725.97470.....	3039.0	none	CBA-NM[a]
2,453,729.61210.....	3053.5	none	CBA-NM[a]
2,453,729.73760.....	3054.0	none	CBA-NM[a]
2,453,729.86210.....	3054.5	none	CBA-NM[a]
2,453,729.98800.....	3055.0	none	CBA-NM[a]
2,453,730.61520.....	3057.5	none	CBA-NM[a]
2,453,730.74040.....	3058.0	none	CBA-NM[a]
2,453,730.86540.....	3058.5	none	CBA-NM[a]
2,453,730.99070.....	3059.0	none	CBA-NM[a]
2,453,731.61840.....	3061.5	none	CBA-NM[a]
2,453,733.50049.....	3069.0	none	CBA-Lesve
2,453,733.61898.....	3069.5	none	CBA-Lesve
2,453,740.39391.....	3096.5	none	CBA-Lesve
2,453,741.52569.....	3101.0	none	CBA-Lesve
2,453,742.52894.....	3105.0	none	CBA-Lesve
2,453,759.33366.....	3172.0	none	CBA-Lesve
2,453,677.82063.....	2847.0	*V*	CBA-Arkansas
2,453,677.95151.....	2847.5	*V*	CBA-Arkansas
2,453,679.951055.....	2855.5	*V*	CBA-Arkansas
2,453,680.82975.....	2859.0	*B*	CBA-Arkansas
2,453,680.95402.....	2859.5	*V*	CBA-Arkansas
2,453,681.83129.....	2863.0	*B*	CBA-Arkansas
2,453,681.83137.....	2863.0	*V*	CBA-Arkansas
2,453,684.84244.....	2875.0	*B*	CBA-Arkansas
2,453,684.84221.....	2875.0	*V*	CBA-Arkansas
2,453,684.96246.....	2875.5	*V*	CBA-Arkansas
2,453,685.84576.....	2879.0	*B*	CBA-Arkansas
2,453,685.96874.....	2879.5	*V*	CBA-Arkansas
2,453,685.84333.....	2879.0	*V*	CBA-Arkansas
2,453,686.84642.....	2883.0	*V*	CBA-Arkansas

[a] Previously published in Krajci (2006).

be found at the CBA Web site.[4] These light curves were used to obtain measurements of the times of minimum for both primary and secondary eclipses that can be found in Table 1.

2.1.2. *USNO Photometry*

Photometric observations obtained at the US Naval Observatory (USNO), Flagstaff Station, were acquired using the 1 m Ritchey-Chrétien telescope. The telescope was equipped with a Tektronix 2048 × 2048 thinned back-illuminated CCD and Johnson *UBV* filters. The camera has a scale of 0.68″ pixel^{-1}, which results in a field of view of 23.2′ × 23.2′.

The field centered on FS Aur was observed on three consecutive nights, 2005 December 4–6 (UT), in the *B*, *V*, and *U* filters, respectively. The resulting light curves are shown in Figures 1–3. Each set of nightly observations was preceded with a set of 20–50 bias frames and 10 dome flats in all three filters. A total of 110, 176, and 73 individual exposures were obtained in the *B*, *V*, and *U* filters, respectively. Each night the field was observed during an 8 hr window, which corresponded to hour angles between −4^h to +4^h. Although each night was devoted to a single filter, at least one set of exposures in all three filters was also acquired each night. The typical seeing during the USNO observing run was between 2″ and 3″.

[4] See http://cba.phys.columbia.edu.

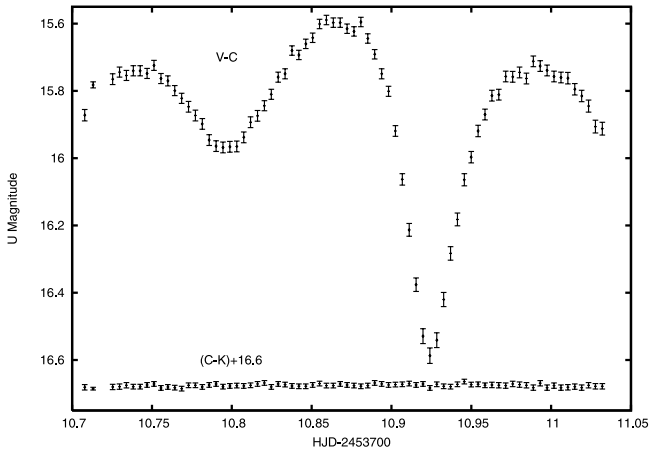

FIG. 1.—*U*-band photometry from 2005 December 6 obtained with the USNO 1 m telescope. The differential *U* magnitudes have been converted to *U* magnitudes using the photometric standard stars for the FS Aur field. The residual magnitudes of the C and K comparison stars are also shown.

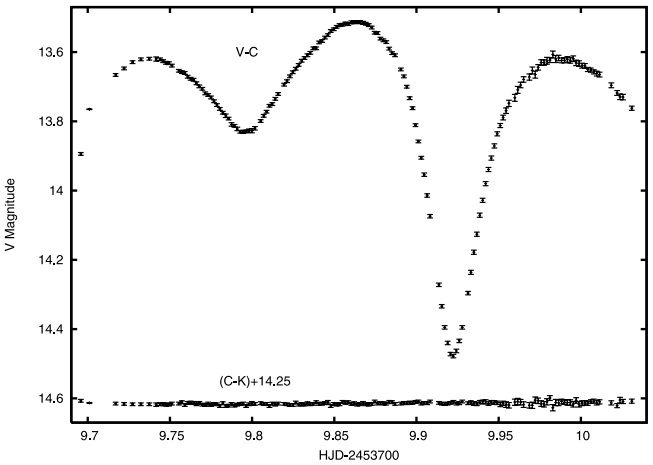

FIG. 3.—*V*-band photometry from 2005 December 5 obtained with the USNO 1 m telescope. The differential *V* magnitudes have been converted to *V* magnitudes using the photometric standard stars for the FS Aur field. The residual magnitudes of the C and K comparison stars are also shown.

2.1.3. *R-Band Photometry*

Time-series differential *R*-band photometry of FS Aur-79 was obtained on 2006 January 2 at the Whispering Pines Observatory in Harrison, Arkansas, using a 0.4 m f4.2 Newtonian telescope with a Johnson *R* filter and SBIG ST-6 CCD camera. The differential *R*-band light curve is shown in Figure 4. The *R* data are very valuable as the extra color information helps reduce the uniqueness problem and limit parameter space in modeling binary light curves, especially those with starspots.

2.1.4. *Photometric Reductions*

All of the CCD images containing photometry data were processed using Cmuniwin.[5] This PC-based software with a graphical user interface was converted from Linux C programs originally developed by Hroch (1998). In short, the images are (1) converted to FITS if necessary, (2) flat-fielded and dark-subtracted if desired, and (3) processed to find stellar targets and photometrically measured using the algorithms of DAOPHOT (Stetson 1987). Then, (4) target lists are pattern matched to identify stars in each image via the algorithm of Groth (1986), and (5) variable, comparison, and check stars are selected to generate differential photometry and light curves.

FS Aur-79 lies close to the cataclysmic variable FS Aur (Robertson et al. 2004), and the field has been observed to establish secondary standard stars (Henden & Honeycutt 1997; A. A. Henden 2006, private communication). Therefore, there are comparison and check stars in the field with standard *U*, *B*, and *V* magnitudes but not *R* as of yet. The magnitude of the comparison star was added to the differential photometry values to yield the magnitudes displayed in Figures 1–3.

2.2. *Spectroscopy*

2.2.1. *WIYN*

Three spectra were obtained on 2006 February 22 UT with the HYDRA Multiple Object Spectrograph on the WIYN[6] 3.5 m telescope at Kitt Peak National Observatory. Table 2 lists the

[5] Available at http://integral.sci.muni.cz/cmunipack/index.html.

[6] The WIYN observatory is a joint facility of the University of Wisconsin-Madison, Indiana University, Yale University, and the National Optical Astronomy Observatory.

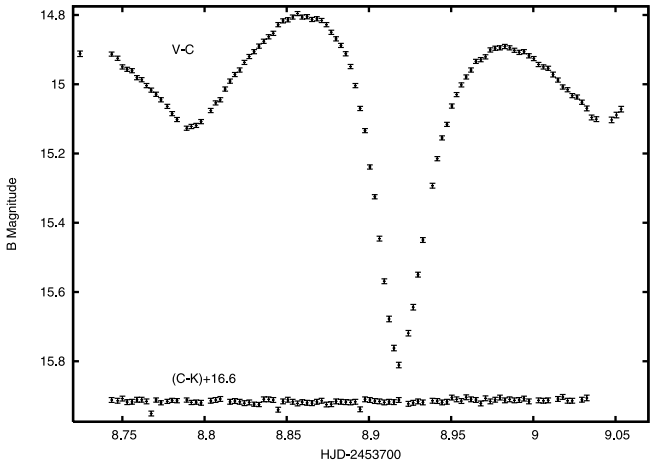

FIG. 2.—*B*-band photometry from 2005 December 4 obtained with the USNO 1 m telescope. The differential *B* magnitudes have been converted to *B* magnitudes using the photometric standard stars for the FS Aur field. The residual magnitudes of the C and K comparison stars are also shown.

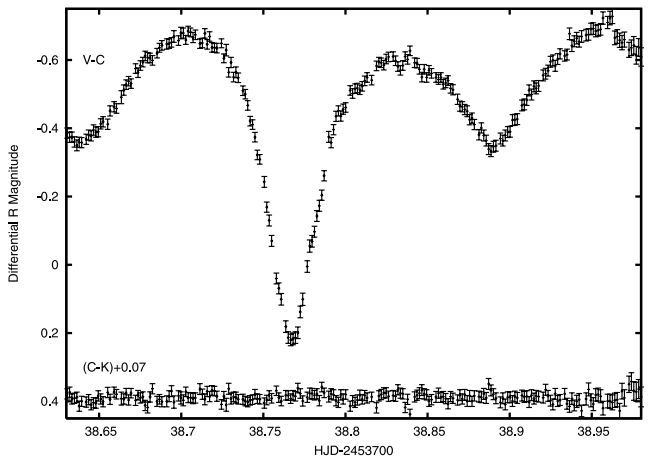

FIG. 4.—*R*-band photometry from 2006 January 2 obtained at Whispering Pines Observatory. The differential *R* magnitudes are shown, since comparison stars have not been calibrated for this field. The residual magnitudes of the C and K comparison stars are also shown.

TABLE 2
WIYN Observations

HJD	Orbital Phase
2,453,788.6109458.....	0.732
2,453,788.6194817.....	0.766
2,453,788.6283672.....	0.801

HJD and orbital phase for each of the spectra obtained. The 600 mm^{-1} grating blazed at 13.9° was used in the first order to obtain a spectrum covering ≈535.0–825.0 nm $pixel^{-1}$ with a resolution of ≈0.14 nm $pixel^{-1}$. Exposure times for the object spectra were 600 s, with wispy cirrus clouds present. Dome-flat and HeArNe arc lamp images were obtained for calibrations to remove individual CCD pixel variations and to convert pixels to wavelengths. Reductions used standard IRAF[7] *onedspec*/*twodspec* procedures to (1) create average flat-field and bias frames (*imcombine*), (2) subtract the bias from object and calibration images, as well as flat-field correct the images (*imarith*), (3) identify, trace, sum, and extract one-dimensional apertures from the two-dimensional CCD images (*apall*), (4) determine and apply the wavelength calibration to object apertures from the HeArNe lamp apertures (*identify*, *refspec*), (5) apply corrections to eliminate the motion of the observatory (*rvcorr*, *dopcor*), and (6) correct the spectra to a flat continuum for relative comparison (*continuum*). Although some unassigned fibers yielded sky, the sky was not extracted or subtracted.

Spectra of FS Aur-62 and FS Aur-63 were also obtained simultaneously through fibers, as these are the comparison stars used in the differential photometry. The photometric calibrations of these stars (Henden & Honeycutt 1997) show that the $B - V$ colors of these stars are 0.412 and 0.450, respectively. To relative flux calibrate the FS Aur-79 spectra we used the spectra of comparison stars with similar $B - V$ colors: LTT 377 ($B - V = 0.48$), LTT 1788 ($B - V = 0.47$), and LTT 2415 ($B - V = 0.40$). We then used spectra of FS Aur-62 and FS Aur-63 with the calibrations of those spectroscopic standards to obtain a relative flux calibration of the FS Aur-79 spectrum using IRAF tasks *standard*, *sensfunc*, and *calibrate*.

The average spectrum of FS Aur-79 is shown in Figure 5 and corresponds to orbital phase ≈0.766. The lines were identified using the line list for K and M stars from Kirkpatrick et al. (1991).

2.2.2. *HET HRS Spectroscopy*

Radial velocity measurements were needed to determine the individual stellar masses. Given the approximately 6 hr orbital period, a visual magnitude of about 14, and the need to acquire high-resolution spectra, a large-aperture telescope was needed. We therefore obtained 10 hr of priority-2 time during 2005 semester B (September through January) on the High Resolution Spectrograph (HRS) at the 9.2 m Hobby-Eberly Telescope (HET) through NOAO. Due to the nature of the HET service observing scheduling only one object spectrum per half night was possible. In order to get as complete a sampling over an orbit as possible, we requested that observations be done as randomly in time as possible over the semester, avoiding consecutive nights at the same time of night due to the approximately 6 hr period of the orbit. The HRS configuration, yielding a resolving power of 15,000 and with a wavelength coverage of approximately 4076–7838 Å, a fiber with an angular diameter on the sky of 3″, one sky fiber, no image slicer, no iodine gas cell, and binning of 2 × 5 for 3.2 pixels per resolving elements, was used. Bias, flat, and Th-Ar comparison lamp frames were also obtained by the night observers for reduction and calibration purposes. Spectral standards were also obtained, giving us the option to relative flux calibrate the spectra. Table 3 lists the details of the 24 HET HRS exposures.

Standard IRAF tasks were used to process the frames into one-dimensional spectra normalized to the continuum. The following reduction steps were used for both the red and blue channels: *zerocombine*, *flatcombine*, *ccdproc* to trim and apply the zero

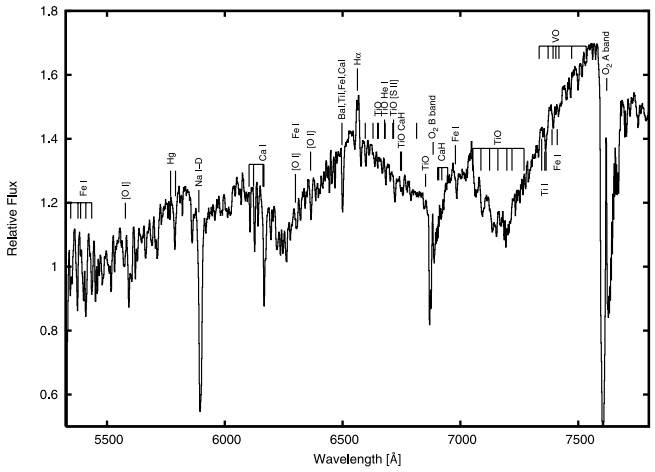

Fig. 5.—The 1.4 Å $pixel^{-1}$ spectrum of FS Aur-79 from 2006 February 21 obtained with the WIYN telescope. This spectrum was obtained at an orbital phase of about 0.76. The major spectral features are labeled and are characteristic of K and M stars.

TABLE 3
HET Observations

UT Date	UT Time	Orbital Phase	Exp (s)	Sky[a]	S/N[b]
2005 Oct 9.....	09:09	0.609	980	S	75
2005 Oct 12.....	08:31	0.465	900	P	124
2005 Oct 20.....	07:48	0.246	900	P	40
2005 Nov 1.....	07:29	0.040	900	P	78
2005 Nov 3.....	07:15	0.976	900	P	82
2005 Nov 11.....	06:40	0.777	900	P	150
2005 Nov 11.....	11:40	0.609	900	P	135
2005 Nov 19.....	06:13	0.599	900	P	140
2005 Nov 19.....	11:22	0.454	900	P	137
2005 Nov 26.....	05:40	0.419	900	S	131
2005 Nov 26.....	10:45	0.263	900	P	153
2005 Dec 10	10:01	0.962	900	P	120
2005 Dec 19	03:47	0.810	1000	P	135
2005 Dec 19	09:15	0.717	900	P	161
2005 Dec 27	03:36	0.674	900	S	114
2005 Dec 28	09:06	0.574	900	S	93
2006 Jan 3.....	02:58	0.478	900	P	114
2006 Jan 11.....	02:21	0.269	900	S	110
2006 Jan 11.....	07:42	0.158	900	S	130
2006 Jan 19.....	07:34	0.030	900	S	...
2006 Jan 20.....	01:51	0.067	900	P	90
2006 Jan 21.....	07:09	0.935	900	P	...
2006 Jan 21.....	07:27	0.984	900	P	72
2006 Jan 29.....	01:35	0.903	900	P	89

[a] S: spectroscopic; P: photometric.
[b] Per resolution element.

[7] IRAF is distributed by the National Optical Astronomy Observatory, which is operated by the Association of Universities for Research in Astronomy, Inc., under cooperative agreement with the National Science Foundation.

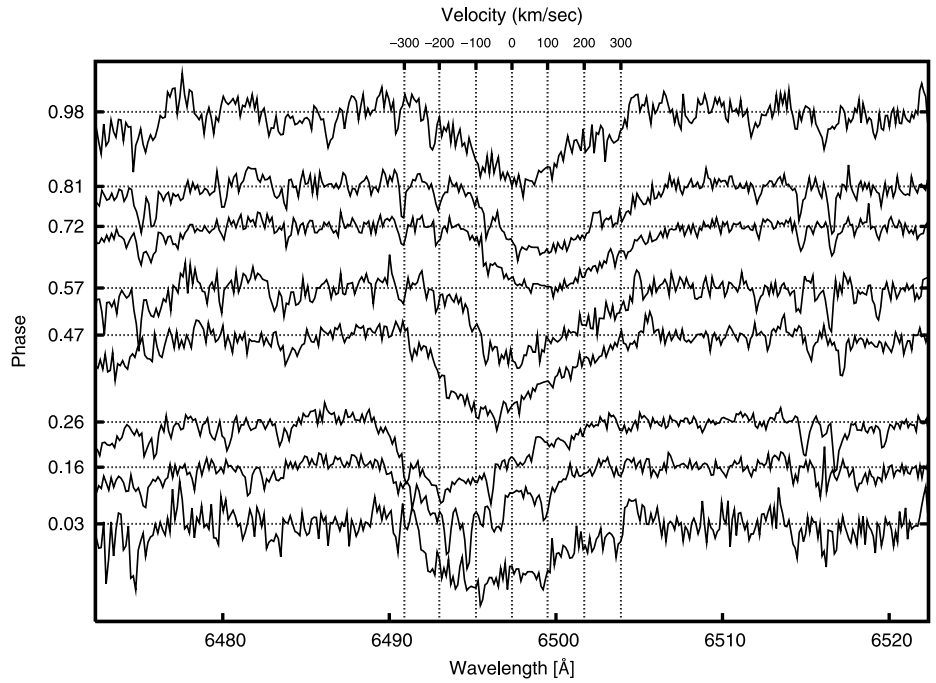

FIG. 6.—Spectra of the Ba I–Ti I–Fe I–Ca I blend at representative orbital phases obtained with the HET HRS (order 94) normalized to the continuum (*horizontal dotted lines*). The velocity scale is for the center-of-mass frame of the binary.

correction, *cosmicrays*, *apall* to find and define the apertures for each spectral order on the red and blue chips, *apscatter* to remove any scattered light, *apflatten* to get a flat-field solution using the combined flat, *ccdproc* to apply the flattening to the spectral frames, and *apall* once again to extract the spectral orders. HET HRS orders 78–145 were extracted, corresponding to spectral coverage from 4200 to 7900 Å. When necessary, sky subtraction was done for those nights near the full moon when the sky background was significant and for those orders that have problematic sky lines (i.e., order 104, Na I D doublet). Wavelength calibration was done for each spectral order of interest using *ident*, *reident*, *refspec*, and *dispcor*. The spectra were then converted to the heliocentric frame of reference using *rvcor* and *dopcor*. The instrumental flux was then normalized to the continuum by using either *contin*, if it could correctly find the continuum, or by doing the continuum fitting interactively using the option under *splot*. Spectra from order 94 are shown in Figure 6, sorted by phase. The main spectral feature in this order is the absorption line blend of

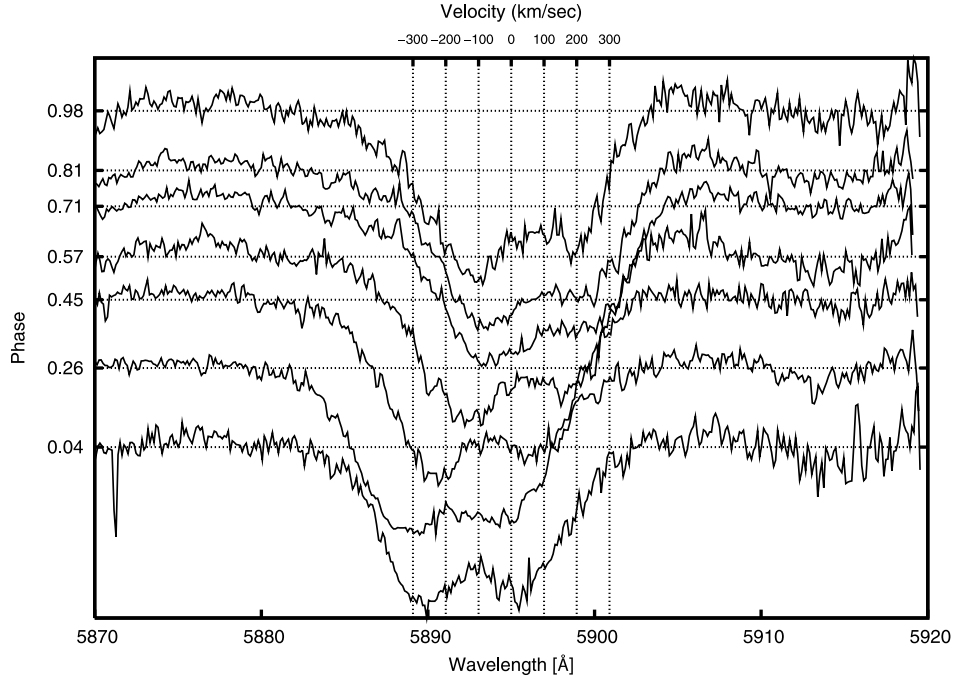

FIG. 7.—Spectra of the Na I D doublet at representative orbital phases obtained with the HET HRS (order 104) normalized to the continuum (*horizontal dotted lines*). The velocity scale is for the center-of-mass frame of the binary.

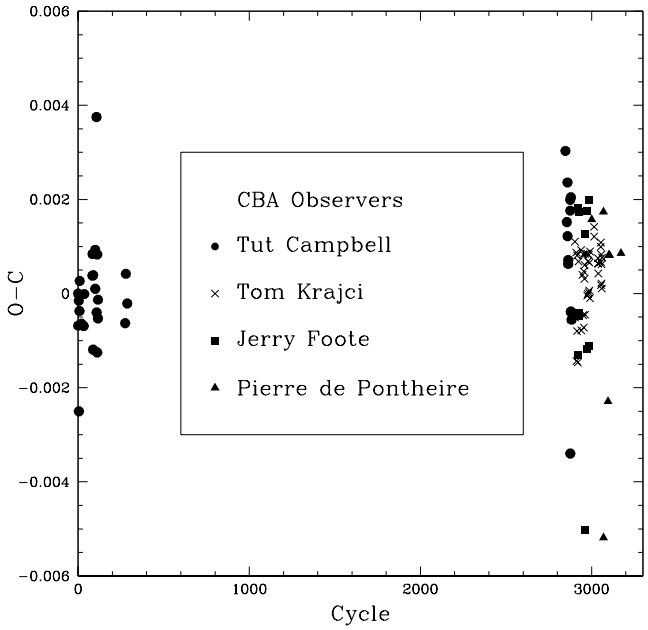

FIG. 8.—Difference between observed and calculated ($O - C$) eclipse timings from CCD photometry of FS Aur-79 obtained by members of the CBA.

Ti I λ6497.689, Ba I λ6498.759, Fe I λ6498.950, Ca I λ6499.694, and Fe I λ6501.681. Figure 7 shows spectra from order 104 containing the Na I D doublet sorted by phase.

3. ANALYSIS

3.1. *Ephemeris*

Both primary and secondary eclipse times of minimum were determined using the method of Kwee & van Woerden (1956) and are listed in Table 1. All of these timings were then used in a linear least-squares fit of the form $T = T_0 + PN$ to refine the period and ephemeris, where T_0 is the Heliocentric Julian Date of primary eclipse minimum (occultation of the more massive, hotter star) from Robertson et al. (2004), N is the orbital cycle since the epoch T_0, P is the orbital period, and T values are the predicted times of primary eclipses. This yielded a period of 0.250816(1) days. The differences between observed eclipses and their calculated timings ($O - C$) based on this new ephemeris, min I = HJD 2,452,963.74445 + 0.250816N, are shown in Figure 8. The fact that ($O - C$) has been approximately zero over four years of photometry would indicate no changes in the orbital period and therefore no indication of any significant mass transfer.

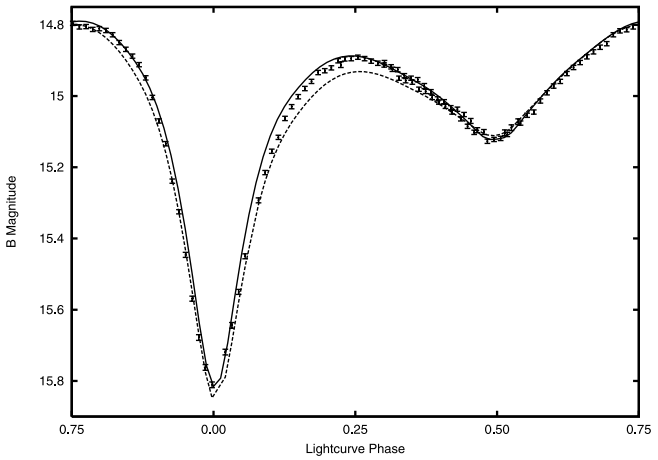

FIG. 10.—Phased B-band photometry from 2005 December 4 obtained with the USNO 1 m telescope. *Solid curve*: Best-fit Nightfall model. *Dashed curve*: BM3 model.

3.2. *Light Curves*

The U, B, V, and R phased light curves of FS Aur-79 are displayed in Figures 9–12. The morphology of these light curves place FS Aur-79 in the category of β Lyrae eclipsing binaries, since the light curves vary continuously and the primary (phase = 0.00) and secondary eclipses (phase = 0.50) are of unequal depths. Table 4 lists the U, B, V, and R magnitudes at primary eclipse, secondary eclipse, max I (phase = 0.25), and max II (phase = 0.75). By comparing the magnitude of the secondary eclipse to the magnitudes during the quadratures we are able to find a lower limit to the magnitude differences between the primary and secondary star, since we do not know if the eclipses are total. The primary star is at least 1.42 mag brighter than the secondary in V and at least 1.33 mag brighter than the secondary in B.

The light curves exhibit the O'Connell effect (unequal maxima) of BY Dra variables, indicating starspots. The amount of the O'Connell effect in each color can be quantified by the difference

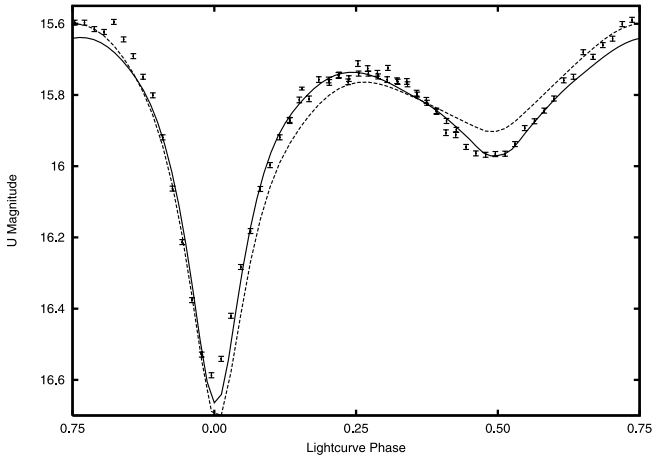

FIG. 9.—Phased U-band photometry from 2005 December 6 obtained with the USNO 1 m telescope. *Solid curve*: Best-fit Nightfall model. *Dashed curve*: BM3 model.

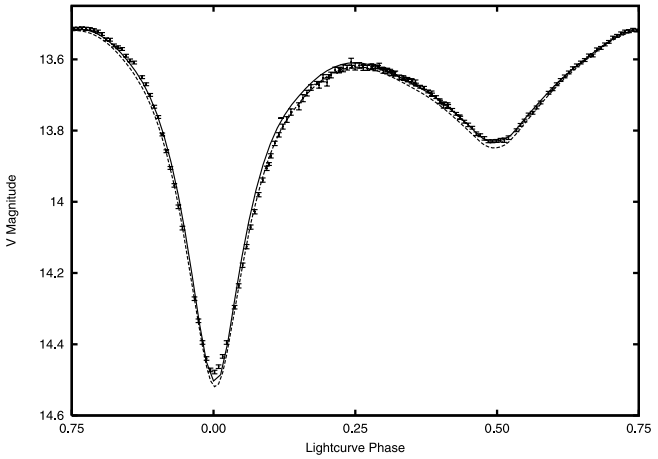

FIG. 11.—Phased V-band photometry from 2005 December 5 obtained with the USNO 1 m telescope. *Solid curve*: Best-fit Nightfall model. *Dashed curve*: BM3 model.

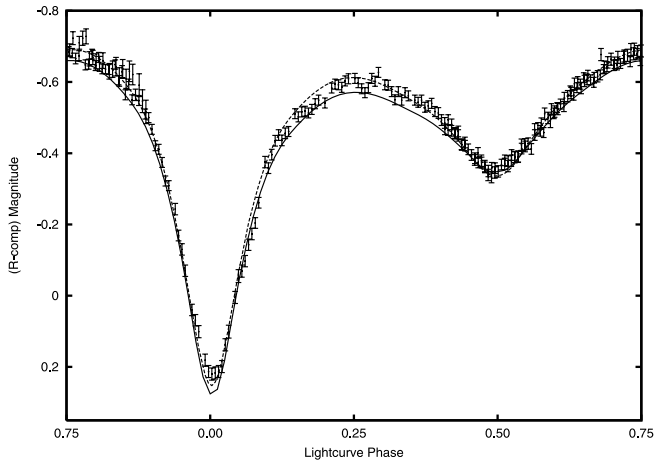

FIG. 12.—Phased *R*-band photometry from 2006 January 2 obtained at Whispering Pines Observatory. *Solid curve*: Best-fit Nightfall model. *Dashed curve*: is the BM3 model.

(Δm) between max II and max I and are listed in Table 5. Also shown in Table 5 are the Δm $U-B$, $B-V$, and $V-R$ colors.

Color curves were computed by first interpolating each light curve to a phase grid with phase increments of 0.0125, then subtracting the light curves of different colors, and therefore also different nights. Figure 13 shows the $U-B$, $B-V$, and differential $V-(R-\mathrm{comp})$ colors with respect to orbital phase. Table 4 includes the $U-B$ and $B-V$ colors at primary eclipse, secondary eclipse, and max I and max II. During secondary eclipse the secondary star is mostly hidden, and the observed color will be for the primary star. $B-V$ during secondary eclipse is about 1.29, which would correspond to a main-sequence star with an effective temperature of around 4100 K and spectral type of about K7. During secondary eclipse, $U-B=0.860$, which would correspond to a main-sequence star with effective temperature of about 4700 K. This $U-B$ excess is an indicator of chromospheric activity (which is also seen in our spectra), and therefore this $U-B$ cannot be used to determine an accurate photospheric temperature (Amado 2003).

The apparent V magnitude of the primary is 13.829, and the $B-V$ color is 1.292. Assuming the primary is a main-sequence star, then the distance modulus $V-M=5.82$, and the distance is about 146 pc (similar to the distance to the Pleiades). Given this distance, reddening and extinction are probably small enough to be ignored.

3.3. *Spectra*

3.3.1. *Spectral Classification*

The WIYN spectrum was obtained when the orbital phase of the system was about 0.76. Figure 14 shows our WIYN spectra, a main-sequence K7 spectrum (star HD 237903), and a main-sequence M1 spectrum (star HD 204445) from the Indo-US Library of Coudé Feed Spectra[8] (Valdes et al. 2004). The K7 and M1 spectra were broadened with a rotational kernel calculated for a $v \sin i$ value of 135 km s^{-1} (approximate rotational speed of FS Aur-79) and a limb-darkening coefficient of 0.6 (see, e.g., Gray 2005, p. 465). The match between the WIYN spectra and the K7 V spectrum is very close between 5200 and 7000 Å. Between 7000 and 7500 Å the WIYN spectrum looks a bit more like an early dM spectrum. But the spectrum between 7000 and 7500 Å is mostly a blend of a K7 V spectrum and an M-type spectrum. Given the uncertainties involved in the atmospheres of cool M-type stars and the lack of absolute-flux calibration available, it is difficult at this time to accurately pinpoint the precise spectral type of the secondary from the WIYN spectrum. Binary modeling in § 3.3 indicates a secondary temperature consistent with an M4 V star, However, the mass and radius found by our binary modeling are more consistent with approximately an M2 V or M3 V star by comparing to the masses and radii determined for YY Gem and CM Dra (Strassmeier et al. 1988). Of all the potential spectroscopic chromospheric indicators that are accessible in our wavelength coverage, such as emission in hydrogen Balmer lines, Ca II H, K emission cores, He I λ5876 absorption or emission core, and Na I D doublet emission cores, this star shows strong emission in Hα along with corresponding emission in Hβ. We therefore estimate the spectral types as dK7e for the primary star and dM3e for the secondary star.

3.3.2. *Velocities*

FS Aur-79 is a single-lined spectroscopic binary, with the lines from the primary star most obvious, and the presence of the lines of the secondary detected by their influence on the line profiles and TiO band strengths. The luminosity difference (in the V band the secondary is at most 0.27 times as bright as the secondary), the short period, and the short exposure times prohibited us from resolving the lines of the secondary.

The γ-velocity (radial velocity of the center of mass of the system relative to the Sun) and the radial velocities of the primary can be measured directly. We first determined the γ-velocity by choosing lines that we were confident were not blends, for example, Ca I lines whose rest wavelengths are 6122.219 and 6162.172 Å. Wavelengths of spectral features of interest were measured using the equivalent width function in the IRAF task *splot*. A sine wave was fit to the wavelength versus orbital phase for these lines that determined the wavelength of the line in the center-of-mass frame relative to the Sun, 6123.94 ± 0.07 and 6163.78 ± 0.11 Å, respectively, resulting in γ-velocities of $+84.3 \pm 3.6$ and $+78.3 \pm 5.4$ km s^{-1}. The chromospheric Hα line does not show any modulation of its wavelength as a function of orbital phase, so it too was used to determine the γ-velocity. Here a line with slope zero was fit to the wavelength versus orbital phase data, resulting in an observed wavelength of 6564.68 ± 0.12 Å and a γ-velocity of $+85.2 \pm 5.5$ km s^{-1}. We conclude that

[8] See http://www.noao.edu/cflib/.

TABLE 4
MAGNITUDES AND COLORS DURING ECLIPSES AND QUADRATURES

Phase	U	B	V	$R-\mathrm{comp}$	$U-B$	$B-V$
0.00 (primary eclipse).....	16.579 ± 0.007	15.811 ± 0.007	14.479 ± 0.06	0.2183 ± 0.015	0.768	1.33
0.25 (max I).....	15.739 ± 0.007	14.892 ± 0.007	13.620 ± 0.06	-0.61155 ± 0.015	0.847	1.272
0.50 (secondary eclipse).....	15.970 ± 0.007	15.121 ± 0.007	13.829 ± 0.06	-0.34813 ± 0.015	0.849	1.292
0.75 (max II).....	15.595 ± 0.007	14.797 ± 0.007	13.517 ± 0.06	-0.68721 ± 0.015	0.798	1.280

TABLE 5
O'Connell Effect

Quantity	Max II − Max I	Color
Δm_U	−0.144	...
Δm_B	−0.095	...
Δm_V	−0.103	...
Δm_R	−0.0757	...
$\Delta m_U - \Delta m_B$	...	−0.049
$\Delta m_B - \Delta m_V$	...	0.008
$\Delta m_V - \Delta m_R$	...	−0.027

the γ-velocity of the system, based on the mean of the values above, is $+82.6 \pm 5.5$ km s^{-1}.

We ran the IRAF cross-correlation task *fxcor* on HET HRS orders 94 through 100, covering a wavelength range of 6070–6535 Å, which contains several strong lines. We used a good S/N spectrum near orbital phase 0.5 as the template. The resulting radial velocity curve had unacceptably large radial velocity errors. The large errors are likely the result of the spectra changing with phase due to not only Doppler shifting but also due to starspot groups, and to a lesser extent the changing relative contributions to the light from the two stars due to the eclipses. By measuring the wavelengths of over a dozen strong absorption lines using the equivalent width function in the IRAF task *splot*, we were not as sensitive to these other effects. Figure 15 shows an example radial velocity curve from the absorption line of the blend at 6500 Å in the center-of-mass frame of the system. The error bars in phase indicate the exposure time for each spectrum, and the error bars in velocity indicate the spectral resolution of the HRS spectra. The maximum radial velocity ($v \sin i$) of the primary is about 125 ± 15 km s^{-1}. Also shown in Figure 15 are the radial velocity curves of both the primary and secondary stars from the best-fit binary model discussed in § 3.4 below.

3.4. *Binary Modeling*

3.4.1. *Optimization*

Light and radial velocity curves were fit simultaneously using the program Nightfall.[9] Nightfall has built-in optimization procedures (simplex and simulated annealing). The temperature of the primary derived from the photometry and spectroscopy was set to 4100 K. The orbital period was set to 0.2508 days. Model atmosphere, detailed reflection, and a square-root limb-darkening law options were enabled. The temperature of the secondary was initially set to a value consistent with a early dM star. We then had Nightfall search parameter space, allowing it to vary the temperature of the secondary, mass ratio, inclination angle, and filling factors for the primary and secondary. Initially only spotless models were computed. Nightfall converged on the values of mass ratio, inclination angle, and filling factor listed in Table 6. Nightfall computes a reduced χ^2 (χ^2_ν) of the simultaneous fit of light and radial velocity curves for the best spotless model of approximately 54.

Spotless models could not reproduce the O'Connell effect, and therefore various starspot models were tried. Starspots are to be expected for stars that have a rotation period of only 0.2508 days (Bopp & Fekel 1977; Young et al. 1987). The temperature of the secondary and the longitude, size, and temperature factor relative to the photosphere (dimming factor) of the circular spot were allowed to vary. The longitude convention used in Nightfall has 0° on the secondary facing L1 and 0° on the primary facing away from L1. An optimized model with a single equatorial spot on the

[9] Available at http://www.hs.uni-hamburg.de/DE/Ins/Per/Wichmann/Nightfall.html.

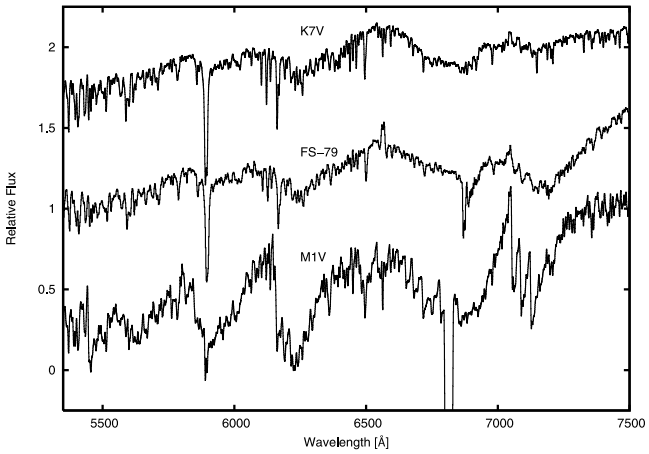

Fig. 14.—The 1.4 Å pixel^{-1} spectrum of FS Aur-79 from 2006 February 21 obtained with the WIYN telescope compared to rotationally broadened ($v \sin i = 135$ km s^{-1}) spectra of K7 V and M1 V stars (Indo-US Library stars HD 237903 and HD 204445 [Valdes et al. 2004]).

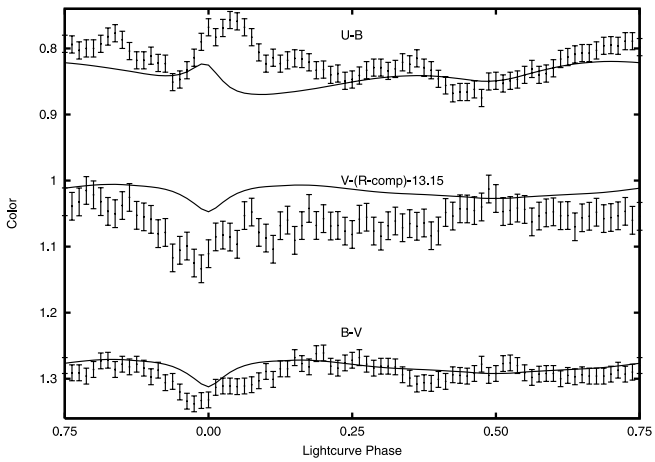

Fig. 13.—Phased $U - B$, $B - V$, and $V - (R - \text{comp})$ light curve. Solid lines represent the best-fit Nightfall model.

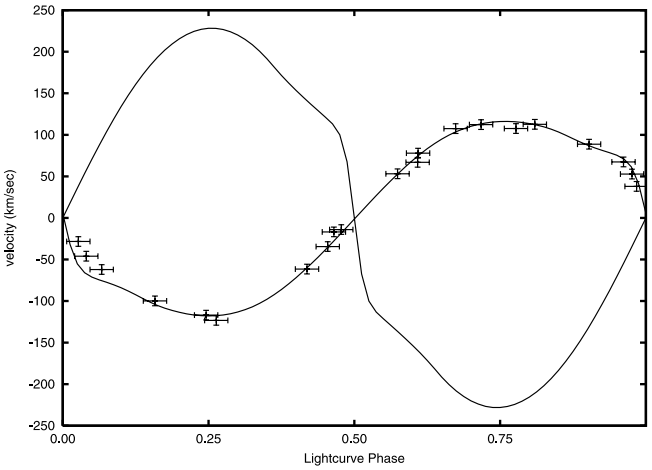

Fig. 15.—Radial velocity curve of the primary star. Solid curves are the model radial velocity curves for the primary and secondary.

TABLE 6
NIGHTFALL MODELS

Parameter	Spotless	One Spot	Three Spot	Uncertainty
Stellar Parameters				
Period (days)[a]	0.251	0.251	0.251	...
i (deg)	83.3	83.3	83.3	±2.3
q (= M_2/M_1)	0.527	0.527	0.527	±0.030
Total mass ($M_\odot$)[a]	0.9	0.9	0.9	±0.1
T_1 (K)[a]	4100	4100	4100	±25
T_2 (K)	3170	3262	3425	±25
Fill factor$_1$	1.00	1.00	1.00	±0.01
Fill factor$_2$	0.950	0.950	0.950	±0.030
Gravity darkening$_1$	0.082	0.082	0.082	...
Gravity darkening$_2$	−0.016	−0.002	0.020	...
Albedo$_1$ = Albedo$_2$	0.5	0.5	0.5	...
Spot(s) Primary (Nightfall Coordinates)				
Longitude-1 (deg)		272	310	...
Latitude-1 (deg)		0	0	...
Radius-1 (deg)		66	55	±10
Dimfactor-1		0.985	0.992	±0.007
Longitude-2 (deg)			210	...
Latitude-2 (deg)			0	...
Radius-2 (deg)			68	±10
Dimfactor-2			0.971	±0.010
Spot(s) Secondary (Nightfall Coordinates)				
Longitude			0	...
Latitude			0	...
Radius (deg)			45	±5
Dimfactor			0.893	±0.050
Output Parameters				
χ^2_ν	54	22	9	...
Mean temperature$_1$ (K)	4106	4089	4062	±25
Mean temperature$_2$ (K)	3170	3262	3365	±25
Mean radius$_1$ ($R_\odot$)	0.673	0.673	0.673	...
Mean radius$_2$ ($R_\odot$)	0.477	0.477	0.477	...
Distance ($R_\odot$)	1.616	1.616	1.616	...
Orbital velocity$_1$ (km s^{-1})	111.61	111.61	111.61	...
Orbital Velocity$_2$ (km s^{-1})	211.83	211.83	211.83	...
M_1 ($M_\odot$)	0.59	0.59	0.59	±0.02
M_2 ($M_\odot$)	0.31	0.31	0.31	±0.09

[a] Held fixed.

secondary resulted in a χ^2_ν of about 22. The best model parameters for a single spot on the secondary are also listed in Table 6.

Although this single-spot model is an improvement over the spotless model, one spot is inadequate to account for the O'Connell effect seen. In other words, the photospheric temperature inhomogeneity is more complex than a single starspot. In fact, what we are modeling as single spots are probably large spot groups. The *UBVR* light curves were fit the best by a three-spot model (Figs. 9–12), one circular spot on the secondary and two circular spots on the primary (Fig. 16). Again, the optimization varied the temperature of the secondary and the longitude, size, and dimming factor for the spots and resulted in a fit with a χ^2_ν of about 9. Table 6 also shows the best-fit parameters for the three-spot model obtained using Nightfall. The uncertainties listed in Table 6 represent the parameter ranges over which the minimum χ^2_ν remains essentially unchanged. We also compared the modelled and observed $U-B$, $B-V$, and $V-(R-\mathrm{comp})$ color curves (Fig. 13). The $B-V$ curve fits the observed values closely at all phases. The $U-B$ curve fits generally well, but the observed data show features that are not reproduced by the model. The $V-(R-\mathrm{comp})$ also fits quite well, but the model seems to have systematic differences compared to the data. The actual spots are probably spot groups that are irregular in shape, and therefore the model cannot reproduce in detail the sunspot group shapes.

The model parameters optimized by Nightfall were cross-checked by modeling with BinaryMaker, version 3.0 (BM3; Bradstreet & Steelman 2002). BM3 assumes the stars to be blackbodies, whereas the stellar atmosphere option was used for the Nightfall models. To achieve a fit similar to that obtained with Nightfall (Figs. 9–12) we had to change the inclination angle slightly and use a secondary temperature 50 K cooler when using BM3; otherwise, the same parameter values were used. The equivalent best-fit three-spot parameters used in BinaryMaker are shown in Table 7. As can be seen in Figures 9–12, the *U* and *B* light curves from BM3 do not fit as well as the Nightfall equivalent, but the *V* and *R* light curves are closer to being identical. We

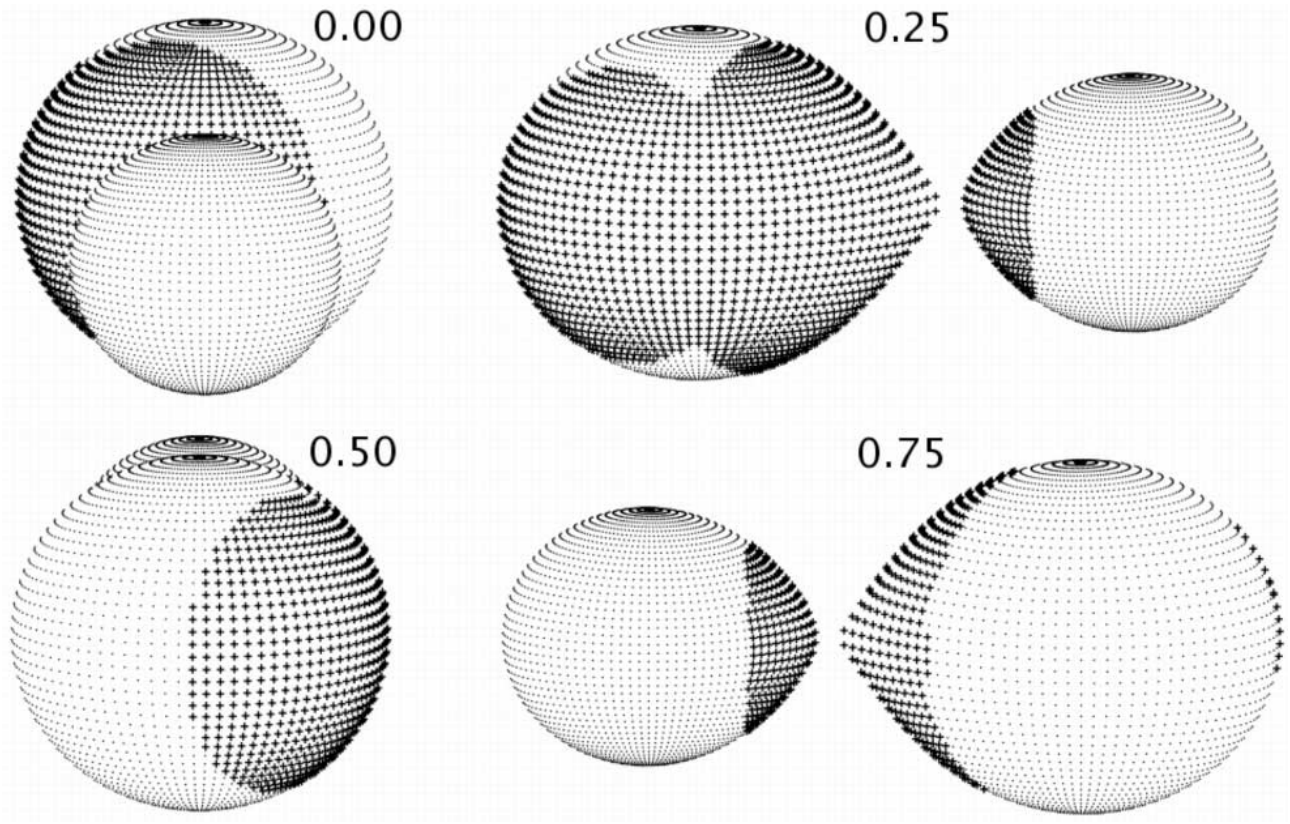

FIG. 16.—Configuration of spots for the best-fit three-spot binary model shown at orbital phases 0.00, 0.25, 0.50, and 0.75.

TABLE 7
BINARYMAKER MODEL

Parameter	Three Spot
Stellar Parameters	
Mass ratio	0.527
Fillout 1	0.0
Fillout 2	−0.01
Temperature 1	4100
Temperature 2	3375
G1 = G2	0.32
X1	0.887
X2	0.973
Reflection 1 = Reflection 2	0.5
Inclination	81
Period	0.251
Spots Primary (BinaryMaker Coordinates)	
Longitude	330
Latitude	90
Spot radius	68.2
Temperature factor	0.97
Longitude	230
Latitude	90
Spot radius	54
Temperature factor	0.99
Spot Secondary (BinaryMaker Coordinates)	
Longitude	0.0
Latitude	90
Spot radius	45
Temperature factor	0.89

attribute these differences to the fact that model atmospheres were used for the Nightfall modeling and blackbodies for the BM3 model.

By simultaneously fitting the U, B, V, and R light curves we improved the likelihood of finding a unique solution. One should interpret the starspots in the model simply as a way to introduce temperature differences on the surfaces of the stars, since one cannot distinguish a cool spot from a hot spot on the opposite side of the system. By comparing the observed and modelled color curves ($U - B$, $B - V$, and $V - R$) in Figure 13, one can see that the model does a good job of reproducing the observed temperature inhomogeneities.

3.4.2. *Spectral Synthesis*

Given the spectral types of the component stars and their observed and predicted radial velocities we have synthesized the Na D line profile for zero and quadrature orbital phases. This provides a qualitative check on the orbital velocity of the secondary star, whose spectral features are not noticeable from visual inspection of the HET HRS spectra. Figure 17 shows the observed and synthesized profiles for order 100. A K7 V spectrum and an M1 V spectrum were normalized to the continuum over the wavelength range of the HET HRS order. The M1 V spectrum was then scaled by a factor of about 0.225 (relative luminosity of an M1 V star in units of a K7 V star's luminosity). The composite spectrum was then normalized to the continuum. The result mimics the line profiles of the sodium doublet, which indicates that the secondary star spectrum is having an observable effect on this spectral feature and that the predicted secondary velocity is probably close to the actual velocity.

4. DISCUSSION

FS Aur-79 represents a very near contact system containing late-type (K–M dwarf) components. Near-contact systems have

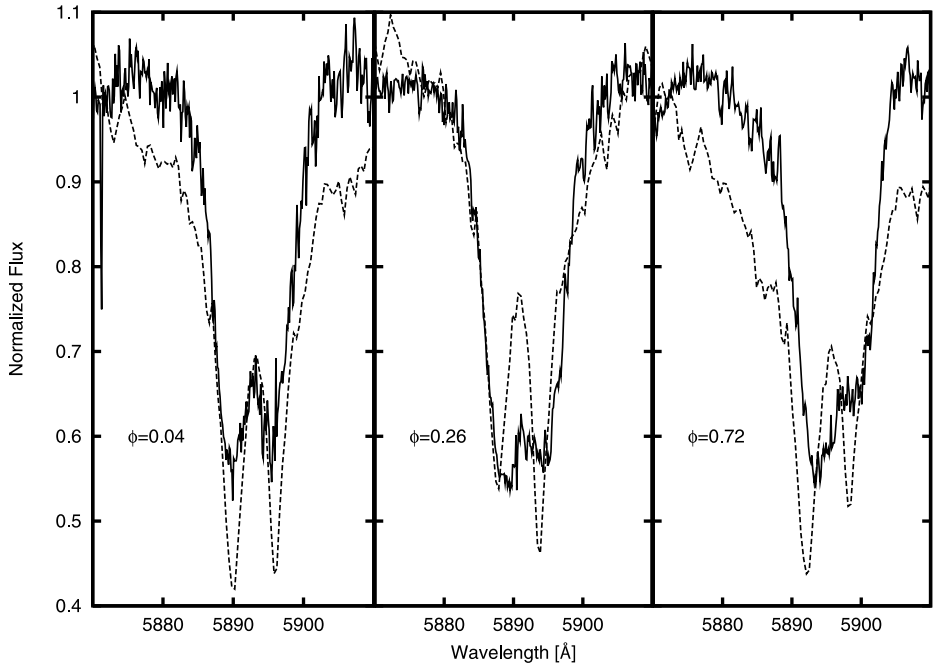

FIG. 17.—Sodium doublet and synthesized profiles for phases 0.0, 0.25, 0.5, and 0.75.

been defined by Shaw (1990), in which the binaries have a period of less than 1 day, show strong tidal interactions, and have surfaces very near one another but not in contact. These stars are related to W UMa type systems and are probable precursors to such systems. W UMa systems have periods less than 1 day, and their light curves show distortions due to their close proximity, similar to near-contact systems. There are no known W UMa type systems with an M star component, so this system represents a unique precursor to such a low-mass W UMa system.

Unlike the W UMa systems, however, the near-contact systems show unequal eclipse depths in their primary and secondary minima. This can be explained with the fact that the stars have different temperatures and are therefore not in contact and hence not in thermal equilibrium, indicative of β Lyrae systems.

There has been some speculation as to the actual existence of W UMa–type systems that are currently not in the contact state due to thermal relaxations (Lucy 1976; Flannery 1976; Wang 1994) or that the stars are somehow able to maintain temperature differences within a contact discontinuity (Shu et al. 1976; Wang 1999). These proposed systems have been referred to as the B-type (apart from W-type and A-type) subclass of W UMa systems. Indeed, it has been shown that some of the observational candidates for the B-type W UMa systems can be the result of spurious effects produced when starspots are not included in light-curve models. Maceroni & van't Veer (1990) showed the effect of modeling a near-contact system with and without starspots. Their results indicated that a spotless contact model could reproduce equally well the light curves of spotted noncontact systems.

Starspots are notorious for introducing ambiguity in light-curve modeling in chromospherically active binaries such as RS CVn and Algols, as well as BY Dra rotational variables, especially when there is only one color-band light curve. Multiwavelength studies, coupled with suitable spectroscopy (i.e., radial velocities and phase-correlated chromospheric activity indicators) can often disentangle multiple light-curve models with the larger number of free parameters introduced by inclusion of starspots.

Close binaries with late-type components are very rare for two reasons. The first and most obvious is their intrinsic faintness and, therefore, observational bias in detecting and observing them in the first place. The other is due to their evolutionary history. Theories of protostellar collapse involving formation of close binary stars with separations 1 AU or less are problematic, as reviewed by Bonnell (2001). Separations of a few AU are possible, however, and further evolution of the binary can lead to short orbital period systems through the loss of angular momentum. Therefore, it takes time for these systems to form.

It is widely known that young stars are rapid rotators and that main-sequence evolution causes a slowing of rotation. The decrease of Ca II H and K emission as a function of age in main-sequence spectral types was clearly demonstrated by Wilson (1963). This leads to an activity versus age relationship among main-sequence stars as their stellar winds, which are coupled to the magnetic field and are forced to corotate with stellar rotation out to large radii, extract angular momentum. The result is that the stars rotate more slowly over time. This in turn reduces the stellar activity level, as the speed of rotation is tied to magnetic dynamo strength. Since the result of extracting angular momentum from a binary system is to tighten the binary orbit, this angular momentum loss mechanism, when operating in a binary system, results in the evolution of the binary to shorter orbital periods. Stepien (1995) has formulated the angular momentum loss via a magnetized wind and the spin-up rate of binaries through their decreasing orbital periods calibrated from observations of the spin-down rates of single stars (Simon et al. 1985). These results show that the timescales for angular momentum loss of rapidly rotating single stars increase substantially for cooler stars and later spectral types. Therefore, the timescale for contact binary formation from initially more widely separated components will increase substantially with later spectral type components. Even the closest in situ formed binaries (2–5 AU) with low enough masses would not have had enough time to reach the near-contact or contact stages within the age of our galaxy. Stepien's (1995) results show that for a binary with two 0.6 $M_{\odot}$ components, angular momentum loss operating over 2.5 Gyr is needed to form a contact binary having an initial orbital period of 2 days. For an initial orbital period of 3.4 days this increases to

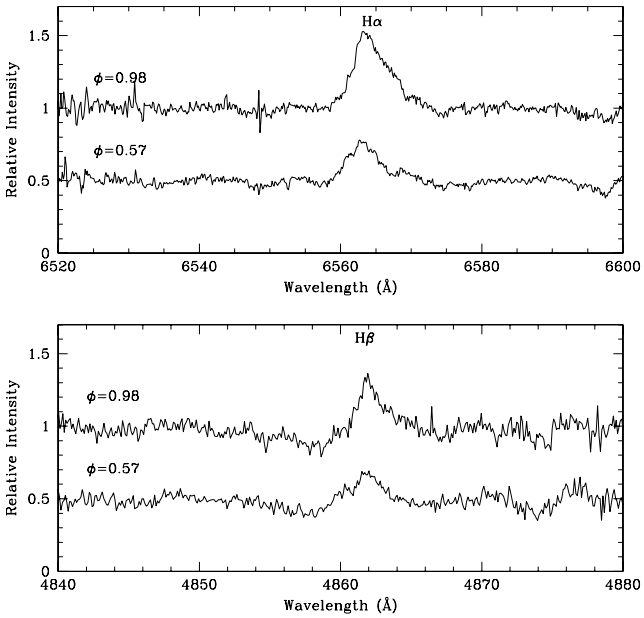

FIG. 18.—Examples of Hα and Hβ in emission lines at phases 0.0 and 0.5.

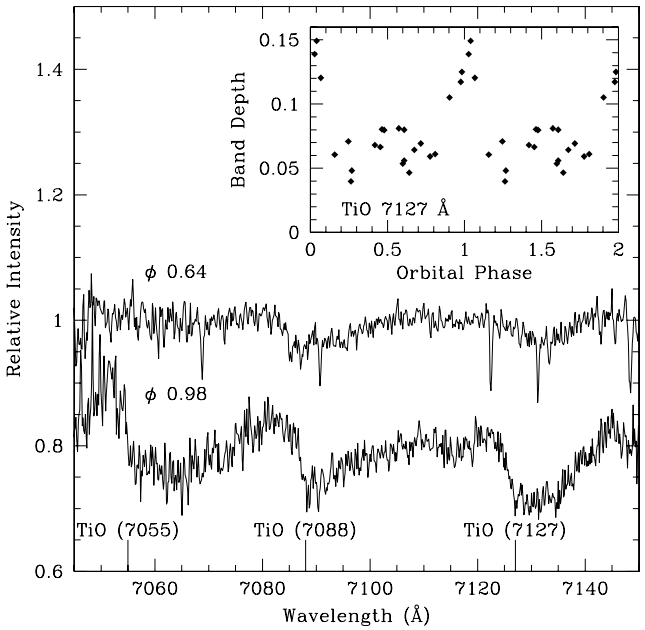

FIG. 19.—TiO bands and band depths.

6 Gyr. The primary star of FS Aur-79 has a mass of approximately 0.6 $M_\odot$ based on its color and spectral type. Our model indicates a mass ratio q of about 0.527, which results in a secondary mass of approximately 0.3 $M_\odot$, which is consistent with a main-sequence star with the modelled temperature of 3425 K. So the Stepien (1995) results should also be roughly applicable to our system. Given the main-sequence lifetimes of our proposed components are ≈56 Gyr and the age of the Galactic disk is ≈12 Gyr (Kaluzny 1990), there has certainly been sufficient time for this binary to reach its current state from a wider initial separation. Of the included binaries in the lists of near-contact binaries (Shaw 1990, Shaw et al. 1996), very few have spectral types later than F and none have a spectral type of M, making this system quite rare.

In fact, there are only a handful of stars thought to be of similar heritage. YY Gem and CM Dra (Strassmeier et al. 1988), CU Cnc (Ribas 2003), BW3 V38 (Maceroni & Montalban 2004), and RE 0618+75 (Jeffries et al. 1993) are potential near-contact siblings along with their contact cousins, for example W Cor (Odell 1996) and VZ Psc (Hrivnak et al. 1995), and those found listed by Hilditch et al. (1988), although none of those contact systems have a dMe component.

It is likely that the tidally enforced synchronous rotation of the stars in this system helps enhance their magnetic activity. Rotation, especially rapid rotation, is a prerequisite for the creation of strong magnetic phenomena seen in stars through an internal dynamo (for a recent review see Donati 2004). FS Aur-79 shows classic signs of chromospheric activity through the emission observed in Hα and Hβ from our spectroscopy (Fig. 18) and starspots inferred from our multiwavelength light-curve modeling. It is therefore likely that this binary is evolving toward contact and has been for a long time.

The temperatures derived by light-curve modeling ($T_1 =$ 4100 K, $T_2 = 3425$ K) are supported by the observed spectra and are a good match (Fig. 14) for a dK7e + dM3e near-contact system. The $B - V$ color of the system also supports these spectral types. The $U - B$ color would seem to be inconsistent with these spectral types, indicating a hotter primary star. However, because of the presumed starspots, the energy output in the UV is likely tainted by chromospheric activity, especially in the U band (Spruit & Weiss 1986; Houdebine et al. 1996). As an independent check of our temperature estimates, the depths of TiO absorption bands have been measured as described by O'Neal et al. (1998). In their paper they obtained empirical relationships between the depth of TiO absorption bands and temperature (their Fig. 1). Measurements of the TiO bands at 7055, 7088, and 7127 Å in our high-resolution spectra are consistent with our temperatures as shown in Figure 19 for TiO (7127 Å).

5. CONCLUSIONS

We find that FS Aur-79 is a near-contact binary system at a distance of ≈146 pc with dK7e and dM3e components separated by 1.62 $R_\odot$. The system has a γ-velocity of $+83 \pm 5.5$ km s^{-1}, with the primary having an orbital velocity around 115 km s^{-1} and the secondary predicted to have an orbital velocity near 210 km s^{-1}. The primary mass, temperature, and radius are ≈0.6 $M_\odot$, 4100 K, and 0.67 $R_\odot$. The secondary mass, temperature, and radius are ≈0.3 $M_\odot$, 3425 K, and 0.48 $R_\odot$. This system is eclipsing with an inclination angle of 83°, with unequal eclipse depths indicating the temperature difference, and unequal quadrature magnitudes indicating the presence of starspots. A $U - B$ excess and H Balmer lines in emission are further evidence of chromospheric activity. The modeling indicates the presence of two major spot regions on the primary and one on the secondary. It is likely that this system has evolved from larger separations through angular momentum loss via stellar winds that are coupled to the magnetic fields from chromospheric activity and forced to corotate out to large radii, thereby extracting angular momentum from the system and tightening the orbit. This likely evolution means this system may become a W UMa system with unique late-type components, which is rare given that the evolution time is so long.

Further study of the high-resolution spectra are under way, including Doppler tomography, deconvolving the primary and secondary spectra, and detailing of the components of emission features as a function of phase. This should provide further information concerning the starspots, the chromospheric regions, and refinement of the stellar masses.

The authors acknowledge the observing time on the HET granted through NOAO. S. J. A. thanks the HET staff for their assistance. J. W. R. would like to thank the members of the CBA, the ever-changing vanguard at the Indiana University RoboScope, and WIYN for the time to take a spectrum with the Hydra-MOS instrument. C. T. acknowledges support under a contract with the Jet Propulsion Laboratory (JPL) funded by NASA through the Michelson Fellowship Program. JPL is managed for NASA by the California Institute of Technology. C. T. would also like to thank Fred Vrba, Hugh Harris, Bob Zavala, and Trudy Tilleman for help and assistance during his USNO 1 m telescope observing runs.

REFERENCES

Amado, P. J. 2003, A&A, 404, 631
Bonnell, I. A. 2001, in IAU Symp. 200, The Formation of Binary Stars, ed. H. Zinnecker & R. D. Mathieu (San Francisco: ASP), 23
Bopp, B. W., & Fekel, F. C. 1977, AJ, 82, 490
Bradstreet, D. H., & Steelman, D. P. 2002, BAAS, 34, 1224
Donati, J.-F. 2004, in IAU Symp. 215, Stellar Rotation, ed. A. Maeder & E. Eenens (San Francisco: ASP), 258
Flannery, B. P. 1976, ApJ, 205, 217
Gray, D. F. 2005, The Observation and Analysis of Stellar Photospheres (3rd ed.; Cambridge: Cambridge Univ. Press)
Groth, E. J. 1986, AJ, 91, 1244
Henden, A. A., & Honeycutt, R. K. 1997, PASP, 109, 441
Hilditch, R. W., King, D. J., & McFarlane, T. M. 1988, MNRAS, 231, 341
Houdebine, E. R., Mathioudakis, M., Doyle, J. G., & Foing, B. H. 1996, A&A, 305, 209
Hrivnak, B. J., Guinan, E. F., & Lu, W. 1995, ApJ, 455, 300
Hroch, F. 1998, in Proc. 29th Conference on Variable Star Research, ed. J. Dusek & M. Zejda (Brno: Masaryk Univ.), 30
Jeffries, R. D., Elliott, K. H., Kellett, B. J., & Bromage, G. E. 1993, MNRAS, 265, 81
Kaluzny, J. 1990, MNRAS, 243, 492
Kirkpatrick, J. D., Henry, T. J., & McCarthy, D. W., Jr. 1991, ApJS, 77, 417
Krajci, T. 2006, Inf. Bull. Variable Stars, 5690, 1
Kwee, K. K., & van Woerden, H. 1956, Bull. Astron. Inst. Netherlands, 12, 327
Lucy, L. B. 1976, ApJ, 205, 208
Maceroni, C., & Montalban, J. 2004, A&A, 426, 577
Maceroni, C., & van't Veer, F. 1990, in Active Close Binaries, ed. C. Ibanoglu (Dordrecht: Kluwer), 309
Odell, A. P. 1996, MNRAS, 282, 373
O'Neal, D., Neff, J. E., & Saar, S. H. 1998, ApJ, 507, 919
Ribas, I. 2003, A&A, 398, 239
Robertson, J. W., Austin, S. J., Campbell, T., & Hoskins, J. 2004, Inf. Bull. Variable Stars, 5536, 1
Shaw, J. S. 1990, in Active Close Binaries, ed. C. Ibanoglu (Dordrecht: Kluwer), 241
Shaw, J. S., Caillault, J. P., & Schmitt, J. H. M. M. 1996, ApJ, 461, 951
Shu, F. H., Lubow, S. H., & Anderson, L. 1976, ApJ, 209, 536
Simon, T., Herbig, G., & Boesgaard, A. M. 1985, ApJ, 293, 551
Spruit, H. C., & Weiss, A. 1986, A&A, 166, 167
Stepien, K. 1995, MNRAS, 274, 1019
Stetson, P. B. 1987, PASP, 99, 191
Strassmeier, K. G., Hall, D. S., Zeilik, M., Nelson, E., Eker, Z., & Fekel, F. C. 1988, A&AS, 72, 291
Valdes, F., Gupta, R., Rose, J. A., Singh, H. P., & Bell, D. J. 2004, ApJS, 152, 251
Wang, J. 1994, ApJ, 434, 277
———. 1999, AJ, 118, 1845
Wilson, O. C. 1963, ApJ, 138, 832
Young, A., Sadjadi, S., & Harlan, E. 1987, ApJ, 314, 272